Title:

# Spectral Induced Polarisation for the Characterisation of Biochar in Sand

Abbreviated title for page heading: SIP of Biochar

Zhan Gao<sup>1</sup> (z.gao@fz-juelich.de), Franz-Hubert Haegel<sup>1</sup>, Johan A. Huisman<sup>1</sup>, Odilia Esser<sup>1</sup>, Egon Zimmermann<sup>2</sup>, Harry Vereecken<sup>1</sup>

<sup>1</sup> Institute of Bio- and Geosciences - Agrosphere (IBG-3), Forschungszentrum Jülich, D-52425 Jülich, Germany

<sup>2</sup> Central Institute of Engineering, Electronics and Analytics - Electronic Systems (ZEA-2), Forschungszentrum Jülich, D-52425 Jülich, Germany

#### **ABSTRACT**

The use of biochar as a soil amendment attracts increasing research interest. However, the lack of methods to detect and monitor biochar in-situ, limits the validation of the fieldscale application of biochar. Spectral induced polarisation (SIP) is a potential tool to characterize biochar in soil. The aim of this study is to investigate the sensitivity of SIP to biochar in sand and to understand how the physicochemical properties of both biochar and the surrounding matrix influence the SIP response. To this end, SIP measurements were conducted on four types of biochar with different mass fractions disseminated in saturated sand as a host media with changing electrical conductivity. In addition, it was investigated how the SIP response depends on the particle size of biochar. The measured SIP data were interpreted by Debye decomposition to obtain values for the peak relaxation time,  $\tau_{peak}$ , total chargeability, M, and normalised total chargeability, M<sub>n</sub>. SIP showed a clear and spectrally differentiated response to the presence of all four types of biochars. M was found to be proportional to the mass fraction of biochars, although relationships varied for each type of biochars.  $\tau_{peak}$  of biochars increased with increasing particle size. Increased electrolyte concentration enhanced M<sub>n</sub> for all biochars, although again the specific response was different for each biochar. In addition, higher electrolyte concentrations decreased  $\tau_{peak}$  for biochars derived from wood through pyrolysis, but did not affect  $\tau_{peak}$  of biochar derived from miscanthus through hydrothermal carbonisation (HTC). It was concluded that the SIP response of pyrolytic biochars resembled that of conductors or semi-conductors, whereas the SIP response of HTC biochar more closely resembled that of clay. Overall, the findings in this study suggest that SIP is a promising method for the detection and characterisation of biochar in soil.

#### INTRODUCTION

Biochar is a product of hydrothermal decomposition, pyrolysis, or gasification of materials from biological origin. It is derived from a wide variety of sources, including wood (Cheng et al. 2014), green waste (Chan et al. 2007), agricultural residues (Demirbas, Pehlivan and Altun 2006), and sewage sludge (Méndez et al. 2012). The chemical and physical properties vary largely between biochar from different types of feedstock and production processes. The chemical composition and the structure depend on the temperature, the contact time and the surrounding medium during carbonisation (Brewer et al. 2014, Suliman et al. 2016, Fuertes et al. 2010). Whereas biochars made by pyrolysis exhibit porous sponge-like structures with pore sizes of about 5 - 50 μm (Jiang et al. 2013, Suliman et al. 2016), chars made by hydrothermal carbonisation are usually much less structured (Fuertes et al. 2010).

Biochar has attracted considerable research interest in the past decade due to its potential value for agricultural and environmental purposes. As a soil amendment, the use of biochar is expected to increase soil organic matter content (Gaskin et al. 2008), enhance soil fertility (Gaskin et al. 2008), and improve water retention (Zhang, Chen and You 2015) and substrate quality of growing media (Nemati et al. 2015). The use of biochar in field trials has been shown to increase crop yield, while greenhouse gas emissions were reduced at the same time (Dong et al. 2013, Mohammadi et al. 2016). Additionally, it is also argued that biochar provides a promising solution for long-term carbon sequestration (Lehmann, Gaunt and Rondon 2006). The aforementioned agronomic and environmental benefits depend on the types and amounts of biochar being used (Butnan et al. 2015, Tryon 1948). Negative impacts of biochar amendments have also been reported. Application of biochar have resulted in a reduction in crop yield (Liu et al. 2017, Van Zwieten et al. 2010) or might even lead to environmental pollution (Kuppusamy et al. 2016) owing to the physical

and chemical properties of specific biochar types or the use of too much biochar. Most biochar studies are focussed on a relatively small scale (laboratory or greenhouse), or they typically describe the effects of a single addition of biochar in the field. The long-term benefits and risks of biochar application are still being discussed (Lehmann et al. 2011, Ogbonnaya and Semple 2013). Clearly, additional studies on the long-term stability of biochars in the field and their sustainable impact on soil properties influencing agricultural production and the environment are urgently required. Although the surface application of biochar is not a new concept, there is a lack of effective methods for long-term field investigations of biochar. Since biochar cannot easily be separated from soil once it has been applied, classical physico-chemical methods require additional effort to obtain information on temporal changes of biochar properties. Consequently, non-invasive methods for identifying, monitoring and characterising biochars at field scale are still required for the systematic and comprehensive assessment of the large-scale application of biochar. Spectral Induced Polarisation (SIP) may provide the required ability for non-invasive characterisation of biochar.

The induced polarisation (IP) of porous materials like soil and rock is caused by charge transport and accumulation in micro-heterogeneous materials in an external electric field (Kemna et al. 2012). It can be observed in time domain by measuring the voltage response after turning off a DC electrical field (TDIP) or in the frequency domain by applying AC electrical fields at multiple frequencies (SIP). TDIP is a well-established geoelectrical method that has been applied in mining exploration for a long time, in particular for detecting conductive materials like ores and graphite (Seigel et al. 2007). Recently, novel applications of SIP in environmental and hydrogeological investigations have appeared due to the improvements of the measurement accuracy and the development of mechanistic models to interpret IP measurements (Kemna et al. 2012, Revil et al. 2012). The SIP

response of a specific material can be described by the frequency-dependent complex electrical conductivity (or resistivity):

$$\sigma^*(\omega) = \sigma'(\omega) + i\sigma''(\omega) = |\sigma^*|e^{i\varphi} = 1/\rho^*$$
 (1)

where  $\omega = 2\pi f$  is the angular frequency and f is the frequency,  $\sigma$ ' and  $\sigma$ " are the real and imaginary part of complex electrical conductivity,  $|\sigma^*|$  is the magnitude of complex conductivity and  $\varphi(\omega)$  is the phase, which is related to the real and imaginary part of the electrical conductivity according to  $\varphi(\omega) = \arctan[\sigma''(\omega) / \sigma'(\omega)]$ .  $\sigma$ ' represents ohmic conduction related to the steady movement of ions in the electrical field.  $\sigma$ " is a measure for the polarisation of the sample which represents the charge storage. The characteristics of SIP spectra can be related to lithological and pedological properties, such as particle size (Leroy et al. 2008, Titov et al. 2002), pore size (Titov et al. 2002, Hördt et al. 2016), fluid salinity (Lesmes and Frye 2001, Slater and Glaser 2003, Weller et al. 2011), hydraulic conductivity (Hördt et al. 2009, Börner, Schopper and Weller 1996), and surface area per pore volume (Börner et al. 1996, Weller et al. 2010).

The polarisation of non-conductive porous materials (e.g. sand, sandstone, clay) in the low frequency range (mHz to kHz) has been widely attributed to the polarisation of the electrical double layer (EDL) including the Stern layer and the diffuse layer (Lesmes and Frye 2001, Revil 2012), membrane polarisation (Marshall and Madden 1959, Titov et al. 2002), or a combination of both (Titov et al. 2002). When conductive materials are present within the porous media, the dipole moment induced by the external electrical field inside the conductive particle should be taken into account (sometimes referred to as electrode polarisation). Wong (1979) established an elaborate mechanistic model to describe the polarisation of disseminated ores assuming spherical particles in the presence of redoxactive ions. In Wong's model, the redox-reaction causes a "leakage current" across the oreelectrolyte interface that leads to imperfect polarisation of the particle. Recently, Misra et

al. (2016) proposed the so-called perfectly polarised interfacial polarisation (PPIP) model without redox reactions to model the interfacial polarisation of uniformly distributed spherical, rod-like, and sheet-like conductive minerals in host media saturated with electrolyte. In contrast to Wong's model that is based on the mobility of ions in the electrolyte surrounding the conductive particles, the PPIP model considers the mobility of the charge carriers both inside the conductive materials and in the host material.

The potential of SIP for detecting and monitoring biochar in soil was shown by previous studies that presented SIP and TDIP measurements on biochar or other porous black carbon materials. For example, Haegel et al. (2012) observed that the SIP response of sand with additions of different pyrolytic biochars or active carbon depended on the feed material and the pyrolysis process. Gurin et al. (2015) made TDIP measurements on disseminated particles of porous artificial graphite and other electronically conductive minerals in sand. Similar polarisation was found for all materials. However, a systematic study on SIP of biochar with respect to the key physical and chemical properties of biochar and the host medium is still required.

At the onset of this study, it was expected that the SIP response associated with biochar might be complex due to the variable physical and chemical properties that may lead to different dominant polarisation processes. In particular, the electrical conductivity of the biochar was expected to play an important role. Gabhi, Kirk and Jia (2017) suggested that the highest heating temperature reached during the carbonisation process of biomass determines the electrical conductivity of biochar. They found that pyrolytic biochar derived from sugar maple, oak and hickory showed a considerable electrical conductivity that depended on the degree of carbonisation as expressed by carbon content and H/C ratio. In contrast, the biochar derived from bamboo was non-conductive. Moreover, Joseph et al. (2015) pointed out that electron exchange between biochar and the soil environment is

likely to occur through redox reactions, because of the presence of a variety of functional groups on the outer and inner surfaces of biochar particles including carboxylic acid and phenolic groups (Suliman et al. 2016). Therefore, the polarisation of conductive particles and the polarisation of the electrical double layer might both occur in the case of biochar, and potentially the polarisation strength is affected by potential redox reactions.

The aim of this work is to determine the sensitivity of SIP to the presence of disseminated biochar in sand under various conditions. In this study, the SIP response of sand-biochar mixtures of four different biochars from different feedstocks and production processes is investigated as a function of (1) variable mass fraction of biochar, (2) variable particle size of biochar and (3) changing electrical conductivity of the electrolyte. SIP measurements are analysed using a Debye decomposition approach, and the links between the SIP response and biochar properties will be discussed.

#### MATERIALS AND METHODS

#### **Materials**

Four types of biochar from different feedstocks and production processes were selected for SIP experiments. Three of them were made by pyrolytic processes from pine wood chips (PW700), pine wood (PW800), and beech wood (BW550). The fourth biochar was obtained by hydrothermal carbonisation (HTC) of Miscanthus giganteus. PW700 was obtained from Carbon Terra GmbH (Augsburg, Germany). The pyrolytic process is characterised by a temperature gradient in a reactor (Schottdorf kiln) from top (input of the feed material) to bottom (output of the biochar). Air is inserted from the bottom leading to gasification at 700 °C in the glowing zone near the output. PW800 was obtained from Pyreg GmbH (Dörth, Germany). It was made by pyrolysis at 800 °C in an auger reactor.

BW550 is a commercial charcoal made by proFagus GmbH (Bodenfelde, Germany) at 550 °C using the Degussa process. HTC was produced by Schlitt GmbH (Antrifttal-Ohmes, Germany) using hydrothermal carbonisation at 200 °C. Different size fractions of PW700 were made by dry sieving of the material as it was obtained. PW800 and BW550 were obtained in larger pieces which were crushed and sieved. HTC is a powdery material which was used as obtained. Key chemical properties of the four biochars are summarised in Tab. 1. Element analyses for PW700 and PW800 were performed on a Vario EL cube (Elementar Analysensysteme GmbH, Langenselbold, Germany). The ash content was determined in a muffle furnace at  $815 \pm 15$  °C. Data for BW550 and HTC were taken from the literature as indicated in Tab. 1. BET specific surface areas were determined by nitrogen adsorption with AUTOSORB-1 (Quantachrome Instruments, Boynton Beach, USA). Samples for BET were pre-treated in vacuum at 100 °C for 2 hours to remove volatile compounds which could contaminate the apparatus. Since biochars are made from natural sources, they are inhomogeneous. Therefore, composition and structure can vary considerably leading to deviations of analytical values of up to 10 % of the mean values given in Tab. 1.

Commercial sand F36 (Quarzwerke Frechen GmbH, Frechen, Germany) was used for the sand-biochar mixtures. It consisted of 99.3 % SiO<sub>2</sub>. The particle diameter of the sand ranges from 0.125 to 0.250 mm. Demineralised water and NaCl p.a. (Merck, Darmstadt, Germany) were used for the electrolyte solutions.

#### **Measurement set-up**

The experimental set-up for SIP measurements on saturated samples is shown in Fig. 1. Two porous bronze disk current electrodes were placed at the top and the bottom of the cylindrical sample holder to inject current. Two cylindrical brass potential electrodes were

inserted in the borings of the side wall of the column. To avoid electrode polarisation, the potential electrodes were retraced into the bores by about 2 times the diameter of potential electrodes (Huisman et al. 2016). A water tank was connected to the bottom of the column for injecting aqueous electrolyte with a multi-channel peristaltic pump (Model 205u, Watson-Marlow, Rommerskirchen, Germany) into the sample holder. Electrolyte was flushed through the samples and the current electrodes from the bottom to the top of the sample.

#### **Sample preparation**

Sand-biochar mixtures with specific mass fraction and particle size of biochar were prepared. Biochar was pre-wetted for 24 hours in 4 mmol L<sup>-1</sup> NaCl electrolyte (with an electrical conductivity of 46 mS m<sup>-1</sup>, which is a typical value for soil solution in temperate climate). The wetted biochar and sand were mixed in a box until a visually homogeneous mixture was obtained (i.e. biochar particles were well distributed in the sand). This mixture was filled into the sample holder in steps of about 1 cm<sup>3</sup> using a wet-packing procedure. The water surface was always kept about 0.5 cm higher than the sand-biochar mixture during the filling procedure. Small air bubbles were removed by stirring slowly with a spoon. This procedure was repeated until the sample holder was filled. Although all sand-biochar mixtures were carefully prepared, deviations of up to 10 % of biochar content may have occurred along the column because the density difference between biochars and sand resulted in a tendency of biochar to separate from sand during wet packing.

After packing, samples were flushed with 4 mmol  $L^{-1}$  NaCl solution for at least 24 hours to equilibrate the electrolyte content in the mixtures and to control the electrical conductivity of the aqueous electrolyte solution ( $\sigma_w$ ). The sample was flushed with a relatively low and constant flow rate of 0.5 L/hour to avoid disturbance of the distribution of biochar. In

addition, samples with 1 and 2 % biochar were further flushed with 6, 8, 12 and 16 mmol  $L^{-1}$  NaCl solutions to investigate the dependence of the complex electrical conductivity on electrolyte concentration. The range of  $\sigma_w$  varied from 46 to 172 mS m<sup>-1</sup> covering a range of salinity that is typically found in agricultural soil. It was difficult to achieve identical electrical conductivity for each of the samples because of ions released from biochar. Flushing was maintained until the measured electrical conductivity of the outflow was stable and close to that of the inflow. The properties of the investigated sand-biochar mixtures are summarised in Tab. 2. The reported pore-volume-normalised surface area,  $S_{por}$ , is usually calculated by:

$$S_{por} = A_s \cdot \rho_g \cdot (1-\phi)/\phi \tag{2}$$

where  $A_s$  is the specific surface area,  $\rho_g$  is the grain density, and  $\phi$  is the porosity of the bulk sample. Due to the low fraction of biochar in the mixture and the large size of the particles of biochar compared to sand, preparation of a representative sample of the sand-biochar mixture for directly determining  $A_s$  of the mixture is not feasible. As an alternative, a mixing law was used to calculate  $S_{por}$  of each sand-biochar mixture by:

$$S_{por} = [(1-\xi) (A_s(sand) \rho_{ds}) + \xi (A_s(BET) \rho_{db})] (1-\phi)/\phi$$
 (3)

where  $A_s(sand)$  is the specific surface area of sand (0.16 m<sup>2</sup> g<sup>-1</sup>),  $A_s(BET)$  is the specific surface area of the considered biochar (Tab. 1),  $\rho_{ds}$  is the grain density of sand (2.6 g cm<sup>-3</sup>),  $\rho_{db}$  is the skeletal density of biochar(1.8 g cm<sup>-3</sup> for PW700, PW800 and BW550, 1.5 g cm<sup>-3</sup> for HTC (Brewer et al. 2014)),  $\phi$  is the porosity of the bulk sample (0.42 to 0.43), and  $\xi$  is the mass fraction of biochar.

#### SIP data acquisition

SIP measurements were made with the electrical impedance spectrometer developed by Zimmermann et al. (2008). The impedance of the sample was measured for 97 frequencies between 1 mHz to 45 kHz. During each of the SIP measurements, alternating sinusoidal current was injected starting from the maximum frequency, decreasing to the minimum frequency and then returning back to the maximum frequency. These repeated measurements are used to check for drift in the SIP measurements. One SIP measurement lasted for 2.5 hours. All experiments were performed in the laboratory at a temperature of  $21 \pm 2$  °C with a temperature variation of less than 0.5 °C during one single measurement. Both  $\sigma$ ' and  $\sigma$ '' were corrected to 20 °C with an empirical factor of 2 % per °C. The measured impedance was converted to the frequency-dependent complex electrical conductivity (Eq. 1) by using the geometrical factor of the four-point electrode arrangement. Electromagnetic (EM) coupling may affect SIP measurements, especially at high frequencies (> 1000 Hz). The main source of EM coupling for the SIP system used here is associated with the contact impedance of the potential electrodes. To reduce this effect, the correction method proposed by Huisman et al. (2016) was applied.

## **Data interpretation**

Debye decomposition (DD) (Nordsiek and Weller 2008, Zisser, Kemna and Nover 2010) was used to analyse the measured SIP data. DD decomposes the complex resistivity  $\rho^*$  into a superposition of N Debye relaxations:

$$\rho^* = \rho_0 \left[ 1 - \sum_{k=1}^N m_k \left( 1 - \frac{1}{1 + i \rho \tau_k} \right) \right] \tag{4}$$

where each of the N Debye spectra is defined by a chargeability  $m_k$  and an associated relaxation time  $\tau_k$ , and  $\rho_0$  is the DC resistivity. The summation of  $m_k$  yields the total chargeability M which is a measure for the area under the phase spectrum.

$$M = \sum_{k=1}^{N} m_k \tag{5}$$

The normalised total chargeability M<sub>n</sub> is obtained by:

$$M_n = M/\rho_0 \tag{6}$$

 $M_n$  was found to be a proxy for the polarisability of the internal surface (Lesmes and Frye 2001, Weller et al. 2010). For materials with a significant frequency dependence of the complex electrical conductivity, M and  $M_n$  better represent the strength of polarisation than values of  $\sigma$ " or  $\varphi$  at a specific frequency. In this study,  $\tau_{peak}$  is determined by the  $\tau_k$  of the maximum  $m_k$ .

A Matlab implementation of Zisser et al. (2010) that uses Tikhonov regularization to constrain the relaxation time distribution was used to perform the Debye decomposition. Hundred relaxation times (N = 100) were used to fit each SIP spectrum in the frequency range of 0.001 to 10000 Hz. More details about the parameter selection with this Matlab implementation package can be found in Kelter et al. (2015).

#### **RESULTS**

Fig. 2 shows  $\sigma'(\omega)$  and  $\sigma''(\omega)$  for sand-biochar mixtures with 2 % biochar and a 4 mmol L<sup>-1</sup> NaCl solution.  $\sigma'(\omega)$  of the different sand-biochar mixtures showed nearly identical values at the lowest frequency. Similar DC conductivity with the same electrolyte concentration suggests that the samples had a comparable formation factor and thus a similar porosity, which provides confidence in the reproducibility of the sample preparation procedure. There was a significant increase of  $\sigma'(\omega)$  with increasing frequency for the biochars from pine wood (PW700 and PW800) resulting from a large polarisation of these samples in the

investigated frequency range (Fig. 2a). A slight increase was found for BW550, while  $\sigma'(\omega)$  only marginally depended on frequency for HTC. The corresponding spectra of  $\sigma''(\omega)$  are shown in Fig. 2b. Overall, all four investigated biochars showed a significant  $\sigma''(\omega)$  response in comparison to pure sand. PW700 and PW800 showed the largest peaks of  $\sigma''(\omega)$ , i.e. the strongest magnitude of polarisation. For these two biochars,  $\sigma''(\omega)$  exhibited the typical shape of a single Cole-Cole curve with a significant peak at approximately 5.5 Hz for PW700 and 0.4 Hz for PW800. BW550 showed a moderate peak at 2 Hz and a secondary peak at approximately 4000 Hz. HTC showed the weakest polarisation, with a slight peak at about 40 Hz.

Fig. 3 shows the effect of the amount of biochar on the SIP spectra of sand-biochar mixtures for biochar PW800 at an electrolyte concentration of 4 mmol L<sup>-1</sup> NaCl. The increasing mass fraction of biochar did not affect the DC conductivity and the position of the peak of  $\sigma$ "( $\omega$ ), but increased  $\sigma$ '( $\omega$ ) at high frequency and produced more pronounced peaks of  $\sigma$ "( $\omega$ ). The measurements with variable mass fraction for other types of biochar showed similar results.

In a next step, the SIP spectra of the sand-biochar mixtures were further examined using Debye decomposition. The total chargeability M obtained from the Debye decomposition showed a linear relationship with the mass fraction of biochar (Fig. 4). Linear regression models where the intercept is fixed to M for the pure sand with the same electrolyte concentration were fitted to the data. The pyrolytic biochars showed a much larger slope than HTC. The deviation of the measured points from the linear fit is mainly a consequence of the heterogeneity of the biochars themselves and problems associated with obtaining a homogeneous biochar distribution in the samples during sample preparation (i.e. the mass fraction is known at the column scale but the SIP measurements are representative of the sand-biochar mixture between the two potential electrodes only).

Repeated measurements showed a deviation of  $\sigma$ "( $\omega$ ) or M of up to 20 % for these reasons. Overall, the results presented in Fig. 4 suggest that M is a potential indicator for the amount of the biochar in soil.

Fig. 5 shows how  $\sigma''(\omega)$  depends on the particle size of the biochar. Sand-biochar mixtures with 1 % biochar of three different size fractions of PW700 and PW800 were investigated at an electrolyte concentration of 4 mmol L<sup>-1</sup> NaCl. The peak frequencies of  $\sigma''(\omega)$  shifted to lower frequencies for increasing grain size. This behaviour was expected since bigger grains usually correspond to longer relaxation times.  $\tau_{peak}$  values from Debye decomposition as a function of the mean biochar particle diameter d are shown in Fig. 6 for PW700 and PW800.

The results presented in Fig. 7 - Fig. 9 show that  $\sigma_w$  had a significant influence on the SIP responses of all types of biochar.  $\sigma'(\omega)$  spectra for 1 % biochar PW700 and HTC with NaCl solutions of different concentrations are presented in Fig. 7a and 7c. The DC conductivity was proportional to  $\sigma_w$  for both samples in accordance with Archie's law (Archie 1942). Fig. 7b and 7d display the corresponding spectra of  $\sigma''(\omega)$ . Generally, both PW700 and HTC showed an increasing trend of  $\sigma''(\omega)$  with rising  $\sigma_w$ . However, the increasing trend was weaker for HTC for high  $\sigma_w$ . The normalised total chargeability  $M_n$  was used to quantify the polarisability as a function of  $\sigma_w$  for all four biochars (Fig. 8).  $M_n$  showed a nearly linear relationship with  $\sigma_w$  for 2 % PW700 and PW800. However,  $M_n$  increased approximately with the square root of  $\sigma_w$  for 2 % BW550. The sand-biochar mixture with 2 % HTC did not show a power-law dependence on  $\sigma_w$ , as already expected from the spectra of  $\sigma''(\omega)$  for 1 % HTC shown in Fig. 7d. In addition, the peak position of  $\sigma''(\omega)$  for 1 % PW700 shifted towards higher frequencies when  $\sigma_w$  increased (Fig. 7b). Accordingly,  $\tau_{peak}$  decreased with  $\sigma_w$  for all pyrolytic chars (PW700, PW800 and BW550)

as illustrated for the mixtures with 2 % biochar samples in Fig. 9. In contrast, the  $\tau_{peak}$  of HTC remained constant with varying  $\sigma_w$  within the measurement accuracy.

#### **DISCUSSION**

This study presents the first systematic SIP measurements on sand-biochar mixtures. The results clearly show that the type of biochar is the main factor that influences the SIP response of sand-biochar mixtures (Fig. 2). Biochars exhibit large variations of the electrical conductivity depending on the degree of carbonisation and associated graphitisation (Gabhi et al. 2017), and materials with larger electrical conductivity are expected to cause stronger polarisation. Generally, a higher heating temperature and a longer heating time during the production process result in a higher degree of carbonisation. With its distinct low carbon content, high H/C and O/C ratios (Tab. 1), and the low production temperature, HTC is expected to be the least electrically conductive biochar. Variations between the three pyrolytic biochars are due to different production temperature and production processes (e.g. presence of air in the case of PW700). Gabhi et al. (2017) reported that the electrical conductivity of biochar derived from the same kind of biomass increased by six orders of magnitude when the biochar samples were exposed to higher temperature. An accompanying moderate increase of the carbon content by 7 % and a reduction of the H/C ratio by 46 % were observed and indicate a higher degree of carbonisation. The increase in conductivity was, however, mainly attributed to a simultaneous increase of graphitisation. Haegel et al. (2012) reported that  $\sigma$ "( $\omega$ ) was negatively correlated with the H content for biochar derived from wood. The same relationship between polarisation and carbon content or H/C was also found for PW700 with different particle sizes but not for PW800 (Fig. 5). However, differences are so small (chargeability between 0.23 and 0.30 for PW700 and between 0.12 and 0.14 for PW800)

that unambiguous correlations could not be obtained. BW550 had the largest carbon content but a higher H/C ratio and a weaker polarisation compared with other pyrolytic biochars derived from wood (PW700 and PW800). Apparently, the graphitisation of BW550 is lower due to the lower production temperature. In addition, BW550 had a lower BET surface area (Tab. 1). This also suggests that the structure of biochar and/or the feedstock may have a significant effect on polarisation. A clear proof of this influence, however, would require systematic investigations on tailored products made from the same feedstock using different pyrolysis temperatures and processes.

Overall, we conclude that there is a general qualitative correspondence between the observed strength of the polarization and the electrical conductivity of biochar inferred from pyrolysis temperature and chemical composition of the four biochars. However, more quantitative data on the electrical conductivity of particulate biochars would be needed to obtain more reliable relationships between the polarisation and the electrical conductivity of biochars. Such data are still lacking for particulate biochars. Previous studies show measurements on larger samples of biochar (Jiang et al. 2013, Gabhi et al. 2017). However, these studies neglected the internal structure (e.g. porosity) which can influence the interpretation of the electrical conductivity of biochars considerably. In our opinion, the determination of the electrical conductivity of solid biochar is challenging, and beyond the scope of this study.

For lack of a more quantitative interpretation approach, the characteristics of the SIP spectra of biochar can qualitatively be compared to those of other materials. Generally, the SIP response of pyrolytic biochar (PW700, PW800 and BW550) shows characteristics of metallic materials, in particular for the pine-wood biochars which were made at higher temperature. For example, the observed SIP phase shift for 2 % silver nanoparticles in sand saturated with NaCl solution exhibits a typical Cole-Cole spectrum with a single maximum

(Joyce et al. 2012) similar to  $\sigma$ " in Fig. 2 for PW800 and PW700. The peak phase of the porous media with 2% silver nanoparticles was about 75 mrad, which is between the 55 mrad for PW800 and 110 mrad for PW700 for the same mass fraction. The phase maximum obtained for the sand-biochar mixture with 2 % BW550 sample (about 18 mrad) is in the same order of magnitude as that from 2 % pyrite in a sand-agar gel matrix (12 - 15 mrad) (Revil et al. 2015). Okay et al. (2014) found that  $\sigma$ "( $\omega$ ) for a mixture of sand and 1 % clay is in the range of  $10^{-6}$  -  $10^{-4}$  S m<sup>-1</sup>, and increases slightly with increasing  $\sigma_w$ , similar to the sand-HTC mixture investigated here. Gurin et al. (2015) found that  $M_n \, \varpropto \, \sigma_w$  for metallic materials (galena, cryptomelane, chalcopyrite, iron) corresponding to our results for pine-wood biochars (Fig. 8).  $M_n$  of HTC showed a smaller increase beyond  $\sigma_w > 80 \text{ mS}$ m<sup>-1</sup> (Fig. 8). Similar behaviour was also observed for sand (Slater and Glaser 2003) and sandstone (Weller et al. 2011). Lesmes and Frye (2001) attributed this behaviour to changes of surface charge density and ionic mobility for non-metallic materials. Increasing electrolyte concentration leads to a stronger association of ions at the mineral-electrolyte interface and a compression of the diffuse double layer which might result in a reduced mobility of the ions due to ion-ion interactions. Weller et al. (2010) argued that conductive particles may support a higher charge density per unit Spor and therefore do not show a saturation effect of  $\sigma$ " with increasing  $\sigma_w$ .

A power law relationship between  $\tau_{peak}$  and particle size was found with exponents approximately equal to 2.7 for PW700 and 2.3 for PW800, which is somewhat larger than the value of 2 reported by Titov et al. (2002) for the membrane polarisation model, and by Leroy et al. (2008) for a Stern layer polarisation model. Interestingly, Wong's model (1979) and the PPIP model (Misra et al. 2016) predict an approximately linear increase of  $\tau_{peak}$  with increasing particle size, and thus seem to be inconsistent with the SIP measurements on biochar in this aspect. Wong's model (1979) and the PPIP model do predict a decrease

of  $\tau_{peak}$  for increasing  $\sigma_w$  for conductive particles, in agreement with the measured results by Gurin et al. (2015) and the behaviour of PW700, PW800 and BW500 in this study (Fig. 9). In contrast, the  $\tau_{peak}$  of HTC did not depend on  $\sigma_w$ , as expected for non-conductive materials. It is important to realize that all available models have been derived for non-porous particles. The effect of an internal porosity and surface area on the SIP response of biochar is unknown, and needs to be investigated in future experimental and modelling studies.

Previous studies have shown that a relationship between SIP parameters and the specific surface area normalised to the pore volume (Spor) exists for various materials including metallic mineral-sand mixtures and clay-sand mixtures (Slater, Ntarlagiannis and Wishart 2006, Weller et al. 2015, Weller et al. 2010). These relationships suggest that  $\sigma$ " at a specific frequency or Mn is approximately linearly dependent on Spor. As the SIP spectra of biochar have a relatively strong frequency dependence, it is more suitable to show Mn rather than  $\sigma$ " as a function of S<sub>por</sub> (Fig. 10). In comparison with previous data sets (e.g. Fig. 3 in Weller et al. (2010)), M<sub>n</sub> values of biochar fall between the values of conductive or semi-conductive materials (iron/magnetite) and clay. PW700 shows the largest M<sub>n</sub>, close to metallic materials, while HTC shows values in a similar range as sand-clay mixtures. PW800 and BW550 show values in between. The results further substantiate that pyrolytic biochars are electronic conductors or semiconductors and that electronic polarisation of biochar particles is the dominating mechanism of polarisation. In contrast, the main mechanism of polarisation for HTC seems to be double layer polarisation, which is further supported by the reduced increase of M<sub>n</sub> with increasing electrolyte concentration (Fig. 8) and the insensitivity of  $\tau_{peak}$  to  $\sigma_w$  (Fig. 9). It should be mentioned that  $S_{por}$  of biochar might be overestimated due to the potential error of BET determination of biochar (Sigmund et al. 2017).

#### **CONCLUSIONS**

This study demonstrates that it is possible to detect and characterise particles of biochar in a sand matrix with SIP. All measured biochars exhibit an obvious frequency-dependent SIP response. The character of the SIP responses of biochar highly depends on the type of biochar. Biochars with a higher degree of carbonisation and graphitisation exhibit larger polarisation. The dominating mechanism of polarisation for pyrolytic biochars seems to be similar to that for conductive or semi-conductive materials. In contrast, double layer polarisation seems to dominate the SIP response for biochar from hydrothermal carbonisation. When mass fractions relevant for practical agricultural applications are used, total chargeability is proportional to the mass fraction of biochar, which may allow the determination of the content of biochar in soil.

The ultimate goal of this research is to develop strategies and techniques for the detection and characterisation of biochar in the environment. Thus, SIP of biochar in soil and under unsaturated conditions should be investigated in future work. Finally, the effectiveness of the SIP method at field scale needs to be tested for this particular application.

#### Acknowledgements

Zhan Gao thanks the Chinese Scholarship Council for financial support of his PhD thesis. The authors gratefully acknowledge the support with the chemical analyses by the Central Institute of Engineering, Electronics and Analytics - Analytics (ZEA-3) of Forschungszentrum Jülich. They also thank Claudia Walraf for the BET measurements. Carbon Terra GmbH, Pyreg GmbH, Santanu Mukherjee (Forschungszentrum Jülich),

Nicolai D. Jablonowski (Forschungszentrum Jülich), Nils Borchard (University of Bonn) and Lutz Breuer (University of Gießen) are thanked for supplying the investigated biochars.

#### REFERENCES

- Archie G. E. 1942. The electrical resistivity log as an aid in determining some reservoir characteristics. Transactions of the American Institute of Mining and Metallurgical Engineers 146, 54-62.
- Bai M., Wilske B., Buegger F., Bruun E. W., Bach M., Frede H. G. and Breuer L. 2014. Biodegradation measurements confirm the predictive value of the O:C-ratio for biochar recalcitrance. Journal of Plant Nutrition and Soil Science 177, 633-637. doi:10.1002/jpln.201300412
- Borchard N., Siemens J., Ladd B., Möller A. and Amelung W. 2014. Application of biochars to sandy and silty soil failed to increase maize yield under common agricultural practice. Soil and Tillage Research 144, 184-194. doi:10.1016/j.still.2014.07.016
- Borchard N., Prost K., Kautz T., Moeller A. and Siemens J. 2012. Sorption of copper (II) and sulphate to different biochars before and after composting with farmyard manure. European Journal of Soil Science 63, 399-409. doi: 10.1111/j.1365-2389.2012.01446.x
- Börner F. D., Schopper J. R. and Weller A. 1996. Evaluation of transport and storage properties in the soil and groundwater zone from induced polarization measurements. Geophysical Prospecting 44, 583-601. doi:10.1111/j.1365-2478.1996.tb00167.x
- Brewer C. E., Chuang V. J., Masiello C. A., Gonnermann H., Gao X. D., Dugan B., Driver L. E., Panzacchi P., Zygourakis K. and Davies C. A. 2014. New approaches to measuring biochar density and porosity. Biomass & Bioenergy 66, 176-185. doi:10.1016/j.biombioe.2014.03.059
- Butnan S., Deenik J. L., Toomsan B., Antal M. J. and Vityakon P. 2015. Biochar characteristics and application rates affecting corn growth and properties of soils

- contrasting in texture and mineralogy. Geoderma 237, 105-116. doi:10.1016/j.geoderma.2014.08.010
- Chan K. Y., Van Zwieten L., Meszaros I., Downie A. and Joseph S. 2007. Agronomic values of greenwaste biochar as a soil amendment. Australian Journal of Soil Research 45, 629-634. doi:10.1071/sr07109
- Cheng C. H., Lin T. P., Lehmann J., Fang L. J., Yang Y. W., Menyailo O. V., Chang K. H. and Lai J. S. 2014. Sorption properties for black carbon (wood char) after long term exposure in soils. Organic Geochemistry 70, 53-61. doi:10.1016/j.orggeochem.2014.02.013
- Demirbas A., Pehlivan E. and Altun T. 2006. Potential evolution of Turkish agricultural residues as bio-gas, bio-char and bio-oil sources. International Journal of Hydrogen Energy 31, 613-620. doi:10.1016/j.jhydene.2005.06.003
- Dong D., Yang M., Wang C., Wang H. L., Li Y., Luo J. F. and Wu W. X. 2013. Responses of methane emissions and rice yield to applications of biochar and straw in a paddy field. Journal of Soils and Sediments 13, 1450-1460. doi:10.1007/s11368-013-0732-0
- Fuertes A. B., Camps Arbestain M., Sevilla M., Maciá-Agulló J. A., Fiol S., López R., Smernik R. J., Aitkenhead W. P., Arce F. and Macias F. 2010. Chemical and structural properties of carbonaceous products obtained by pyrolysis and hydrothermal carbonisation of corn stover. Australian Journal of Soil Research 48, 618-626. doi:10.1071/SR10010
- Gabhi R. S., Kirk D. W. and Jia C. Q. 2017. Preliminary investigation of electrical conductivity of monolithic biochar. Carbon 116, 435-442. doi:10.1016/j.carbon.2017.01.069

- Gaskin J. W., Steiner C., Harris K., Das K. C. and Bibens B. 2008. Effect of low-temperature pyrolysis conditions on biochar for agricultural use. Transactions of the ASABE 51, 2061-2069.
- Gurin G., Titov K., Ilyin Y. and Tarasov A. 2015. Induced polarization of disseminated electronically conductive minerals: a semi-empirical model. Geophysical Journal International 200, 1555-1565. doi:10.1093/gji/ggu490
- Haegel F.-H., Zimmermann E., Jablonowski N. D., Esser O., Huisman J. A. and Vereecken
  H. 2012. Application of Spectral Induced Polarization and Electrical Impedance
  Tomography on Mixtures of Biochars and Active Carbons with Sand. Proceedings of
  the 25th Symposium on the Application of Geophysics to Engineering and
  Environmental Problems 25, 586-597. doi:10.4133/1.4721883
- Hördt A., Bairlein K., Bielefeld A., Bücker M., Kuhn E., Nordsiek S. and Stebner H. 2016. The dependence of induced polarization on fluid salinity and pH, studied with an extended model of membrane polarization. Journal of Applied Geophysics 135, 408-417. doi:10.1016/j.jappgeo.2016.02.007
- Hördt A., Druiventak A., Blaschek R., Binot F., Kemna A., Kreye P. and Zisser N. 2009. Case histories of hydraulic conductivity estimation with induced polarization at the field scale. Near Surface Geophysics 7, 529-545.
- Huisman J. A., Zimmermann E., Esser O., Haegel F. -H., Treichel A. and Vereecken H. 2016. Evaluation of a novel correction procedure to remove electrode impedance effects from broadband SIP measurements. Journal of Applied Geophysics 135, 466-473. doi:10.1016/j.jappgeo.2015.11.008
- Jiang J. H., Zhang L., Wang X. Y., Holm N., Rajagopalan K., Chen F. L. and Ma S. G. 2013. Highly ordered macroporous woody biochar with ultra-high carbon content as

- supercapacitor electrodes. Electrochimica Acta 113, 481-489. doi:10.1016/j.electacta.2013.09.121
- Joseph S., Husson O., Graber E. R., van Zwieten L., Taherymoosavi S., Thomas T., Nielsen S., Ye J., Pan G. X., Chia C., Munroe P., Allen J., Lin Y., Fan X. R. and Donne S. 2015. The electrochemical properties of biochars and how they affect soil redox properties and processes. Agronomy-Basel 5, 322-340. doi:10.3390/agronomy5030322
- Joyce R. A., Glaser D. R., Werkema D. D. and Atekwana E. A. 2012. Spectral induced polarization response to nanoparticles in a saturated sand matrix. Journal of Applied Geophysics 77, 63-71. doi:10.1016/j.jappgeo.2011.11.009
- Kelter M., Huisman J. A., Zimmermann E., Kemna A. and Vereecken H. 2015.

  Quantitative imaging of spectral electrical properties of variably saturated soil columns.

  Journal of Applied Geophysics 123, 333-344. doi:10.1016/j.jappgeo.2015.09.001
- Kemna A., Binley A., Cassiani G., Niederleithinger E., Revil A., Slater L., Williams K. H., Orozco A. F., Haegel F. -H., Hördt A., Kruschwitz S., Leroux V., Titov K. and Zimmermann E. 2012. An overview of the spectral induced polarization method for near-surface applications. Near Surface Geophysics 10, 453-468. doi:10.3997/1873-0604.2012027
- Kuppusamy S., Thavamani P., Megharaj M., Venkateswarlu K. and Naidu R. 2016.

  Agronomic and remedial benefits and risks of applying biochar to soil: Current knowledge and future research directions. Environment International 87, 1-12. doi:10.1016/j.envint.2015.10.018
- Lehmann J., Gaunt J. and Rondon M. 2006. Bio-char sequestration in terrestrial ecosystems a review. Mitigation and Adaptation Strategies for Global Change 11, 403-427. doi:10.1007/s11027-005-9006-5

- Lehmann J., Rillig M. C., Thies J., Masiello C. A., Hockaday W. C. and Crowley D. 2011.

  Biochar effects on soil biota a review. Soil Biology and Biochemistry 43, 1812-1836.

  doi:10.1016/j.soilbio.2011.04.022
- Leroy P., Revil A., Kemna A., Cosenza P. and Ghorbani A. 2008. Complex conductivity of water-saturated packs of glass beads. Journal of Colloid and Interface Science 321, 103-117. doi:10.1016/j.jcis.2007.12.031
- Lesmes D. P. and Frye K. M. 2001. Influence of pore fluid chemistry on the complex conductivity and induced polarization responses of Berea sandstone. Journal of Geophysical Research-Solid Earth 106, 4079-4090. doi:10.1029/2000jb900392
- Liu C., Liu F., Ravnskov S., Rubaek G. H., Sun Z. and Andersen M. N. 2017. Impact of Wood Biochar and Its Interactions with Mycorrhizal Fungi, Phosphorus Fertilization and Irrigation Strategies on Potato Growth. Journal of Agronomy and Crop Science 203, 131-145. doi:10.1111/jac.12185
- Marshall D. J. and Madden T. R. 1959. Induced polarization, a study of its causes. Geophysics 24, 790-816.
- Méndez A., Gómez A., Paz-Ferreiro J. and Gascó G. 2012. Effects of sewage sludge biochar on plant metal availability after application to a Mediterranean soil. Chemosphere 89, 1354-1359. doi:10.1016/j.chemosphere.2012.05.092
- Misra S., Torres-Verdin C., Revil A., Rasmus J. and Homan D. 2016. Interfacial polarization of disseminated conductive minerals in absence of redox-active species Part 1: Mechanistic model and validation. Geophysics 81, E139-E157. doi:10.1190/geo2015-0346.1
- Mohammadi A., Cowie A., Mai T. L. A., de la Rosa R. A., Kristiansen P., Brandao M. and Joseph S. 2016. Biochar use for climate-change mitigation in rice cropping systems. Journal of Cleaner Production 116, 61-70. doi:10.1016/j.jclepro.2015.12.083

- Nemati M. R., Simard F., Fortin J. -P. and Beaudoin J. 2015. Potential use of biochar in growing media. Vadose Zone Journal 14, 6. doi:10.2136/vzj2014.06.0074
- Nordsiek S. and Weller A. 2008. A new approach to fitting induced-polarization spectra. Geophysics 73, F235-F245. doi:10.1190/1.2987412
- Ogbonnaya U. and Semple K. T. 2013. Impact of biochar on organic contaminants in soil: a tool for mitigating risk? Agronomy 3, 349-375. doi:10.3390/agronomy3020349
- Okay G., Leroy P., Ghorbani A., Cosenza P., Camerlynck C., Cabrera J., Florsch N. and Revil A. 2014. Spectral induced polarization of clay-sand mixtures: Experiments and modeling. Geophysics 79, E353-E375. doi:10.1190/geo2013-0347.1
- Revil A. 2012. Spectral induced polarization of shaly sands: Influence of the electrical double layer. Water Resources Research 48, W02517. doi:10.1029/2011wr011260
- Revil A., Aal G. Z. A., Atekwana E. A., Mao D. Q. and Florsch N. 2015. Induced polarization response of porous media with metallic particles Part 2: Comparison with a broad database of experimental data. Geophysics 80, D539-D552. doi:10.1190/geo2014-0578.1
- Revil A., Karaoulis M., Johnson T. and Kemna A. 2012. Review: Some low-frequency electrical methods for subsurface characterization and monitoring in hydrogeology. Hydrogeology Journal 20, 617-658. doi:10.1007/s10040-011-0819-x
- Seigel H., Nabighian M., Parasnis D. S. and Vozoff K. 2007. The early history of the induced polarization method. The Leading Edge 26, 312-321. doi: 10.1190/1.2715054
- Sigmund G., Hüffer T., Hofmann T. and Kah M. 2017. Biochar total surface area and total pore volume determined by N<sub>2</sub> and CO<sub>2</sub> physisorption are strongly influenced by degassing temperature. Science of the Total Environment 580, 770-775. doi:10.1016/j.scitotenv.2016.12.023

- Slater L., Ntarlagiannis D. and Wishart D. 2006. On the relationship between induced polarization and surface area in metal-sand and clay-sand mixtures. Geophysics 71, A1-A5. doi:10.1190/1.2187707
- Slater L. D. and Glaser D. R. 2003. Controls on induced polarization in sandy unconsolidated sediments and application to aquifer characterization. Geophysics 68, 1547-1558. doi:10.1190/1.1620628
- Suliman W., Harsh J. B., Abu-Lail N. I., Fortuna A. M., Dallmeyer I. and Garcia-Perez M. 2016. Influence of feedstock source and pyrolysis temperature on biochar bulk and surface properties. Biomass and Bioenergy 84, 37-48. doi:10.1016/j.biombioe.2015.11.010
- Titov K., Komarov V., Tarasov V. and Levitski A. 2002. Theoretical and experimental study of time domain-induced polarization in water-saturated sands. Journal of Applied Geophysics 50, 417-433. doi:10.1016/s0926-9851(02)00168-4
- Tryon E. H. 1948. Effect of charcoal on certain physical, chemical, and biological properties of forest soils. Ecological Monographs 18, 81-115. doi:10.2307/1948629
- Van Zwieten L., Kimber S., Morris S., Chan K. Y., Downie A., Rust J., Joseph S. and Cowie A. 2010. Effects of biochar from slow pyrolysis of papermill waste on agronomic performance and soil fertility. Plant and Soil 327, 235-246. doi:10.1007/s11104-009-0050-x
- Weller A., Breede K., Slater L. and Nordsiek S. 2011. Effect of changing water salinity on complex conductivity spectra of sandstones. Geophysics 76, F315-F327. doi:10.1190/geo2011-0072.1
- Weller A., Slater L., Huisman J. A., Esser O. and Haegel F. -H. 2015. On the specific polarizability of sands and sand-clay mixtures. Geophysics 80, A57-A61. doi:10.1190/geo2014-0509.1

- Weller A., Slater L., Nordsiek S. and Ntarlagiannis D. 2010. On the estimation of specific surface per unit pore volume from induced polarization: A robust empirical relation fits multiple data sets. Geophysics 75, WA105-WA112. doi:10.1190/1.3471577
- Wong J. 1979. An electrochemical model of the induced-polarization phenomenon in disseminated sulfide ores. Geophysics 44, 1245-1265. doi:10.1190/1.1441005
- Zhang J., Chen Q. and You C. F. 2016. Biochar effect on water evaporation and hydraulic conductivity in sandy soil. Pedosphere 26, 265-272. doi:10.1016/s1002-0160(15)60041-8
- Zimmermann E., Kemna A., Berwix J., Glaas W., Münch H. M. and Huisman J. A. 2008.

  A high-accuracy impedance spectrometer for measuring sediments with low polarizability. Measurement Science and Technology 19, 105603. doi:10.1088/0957-0233/19/10/105603
- Zisser N., Kemna A. and Nover G. 2010. Relationship between low-frequency electrical properties and hydraulic permeability of low-permeability sandstones. Geophysics 75, E131-E141. doi:10.1190/1.3413260

# **List of Figures**

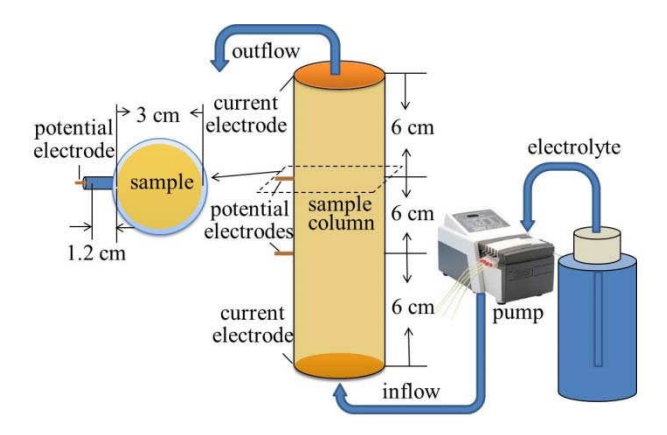


Figure 1. Sketch of the experimental set-up.

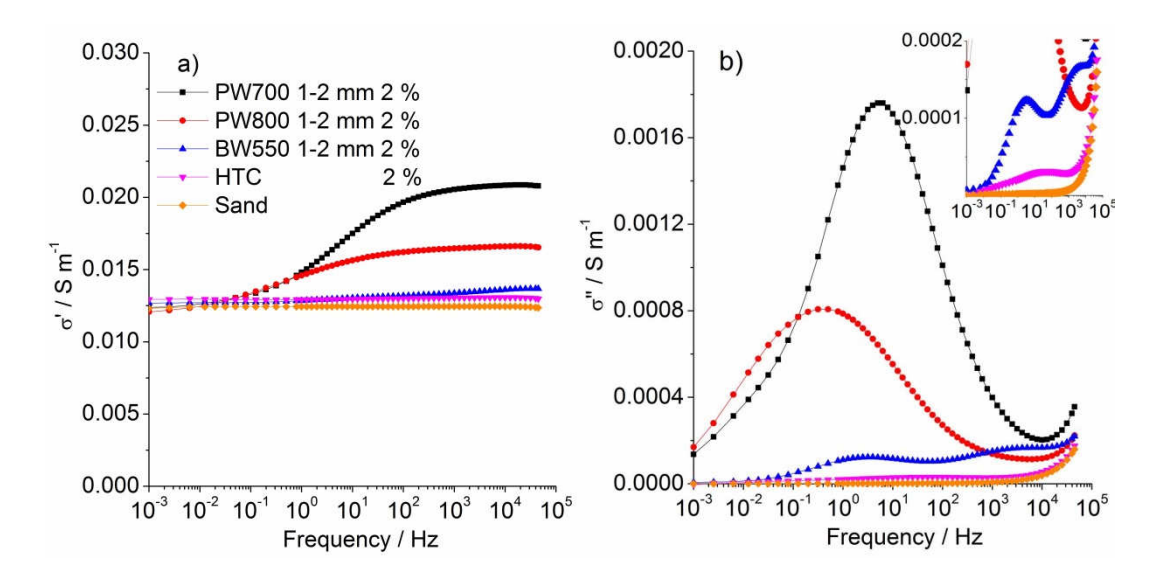


Figure 2. Complex conductivity of mixtures of sand and 2 % of different biochars (4 mmol L<sup>-1</sup> NaCl); a) real part, b) imaginary part. The inset expands the y-scale to highlight the spectra of samples with low polarisation.

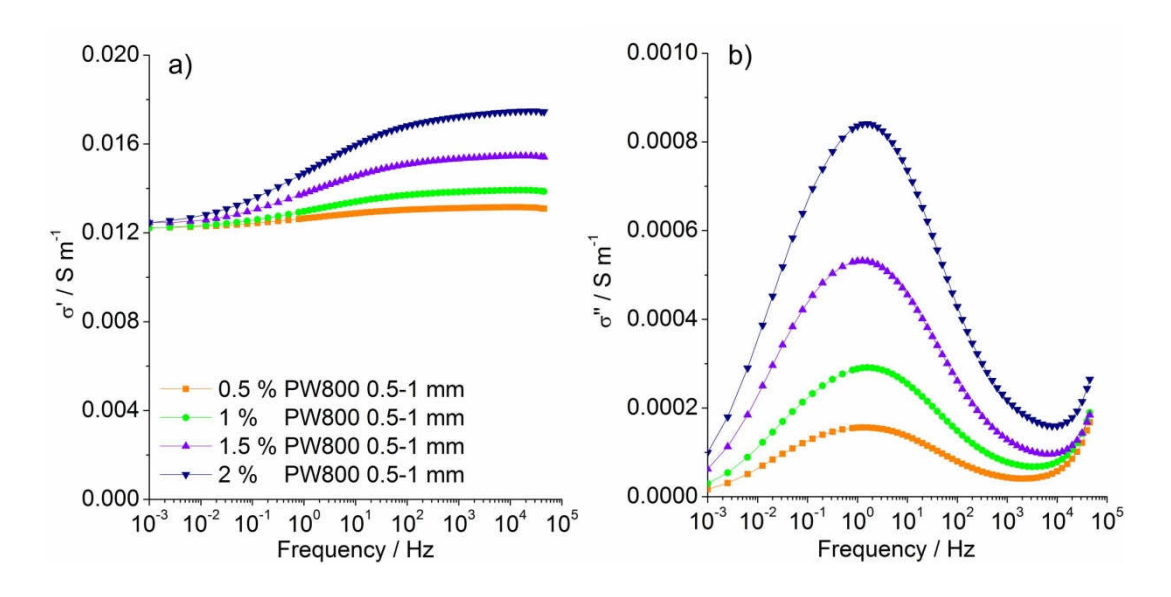


Figure 3. Complex conductivity of PW800 with different mass fraction of biochar (4 mmol L<sup>-1</sup> NaCl); a) real part, b) imaginary part.

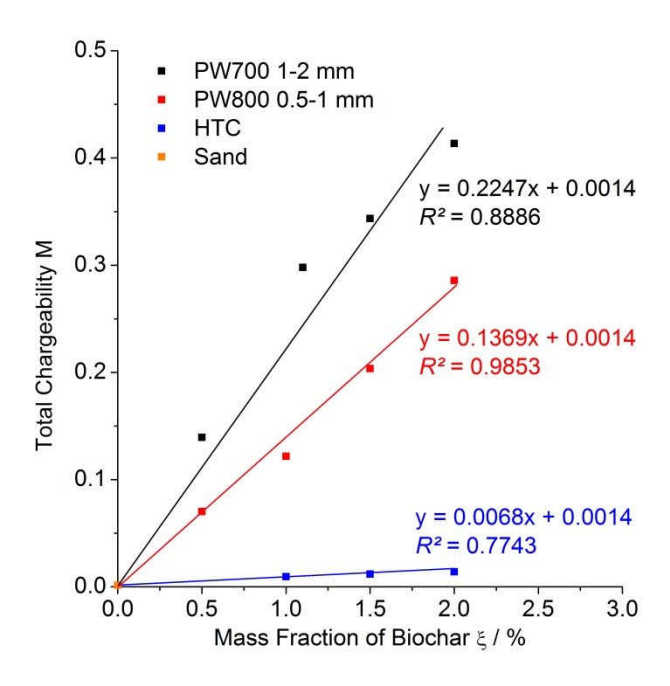


Figure 4. Total chargeability M of PW700, PW800 and HTC as a function of mass fraction of biochar in sand-biochar mixtures (4 mmol  $\rm L^{-1}$  NaCl).

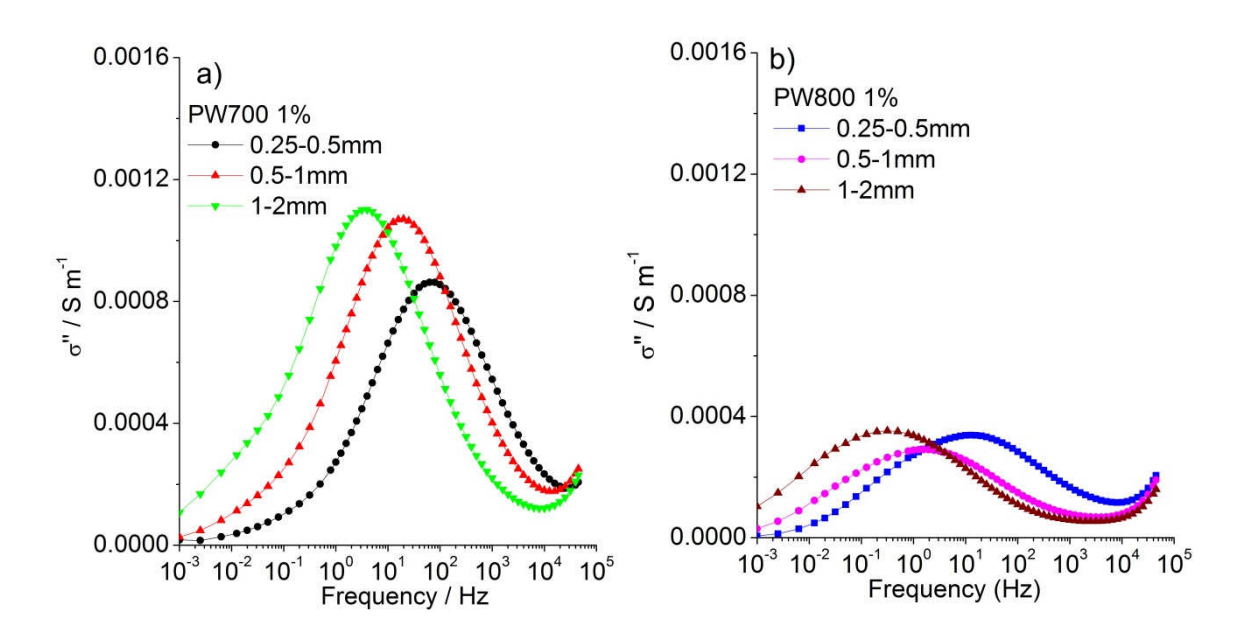


Figure 5. Imaginary part of the complex conductivity of a) PW700 and b) PW800 with different particle size of biochar in sand-biochar mixtures (4 mmol L<sup>-1</sup> NaCl).

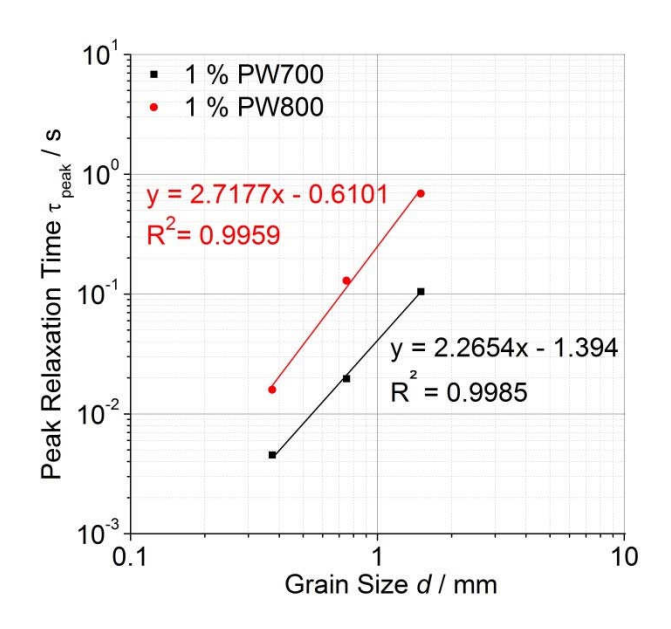


Figure 6. Peak relaxation time  $\tau_{peak}$  of PW700 and PW800 as a function of grain size d of biochar in sand-biochar mixtures (4 mmol L<sup>-1</sup> NaCl).

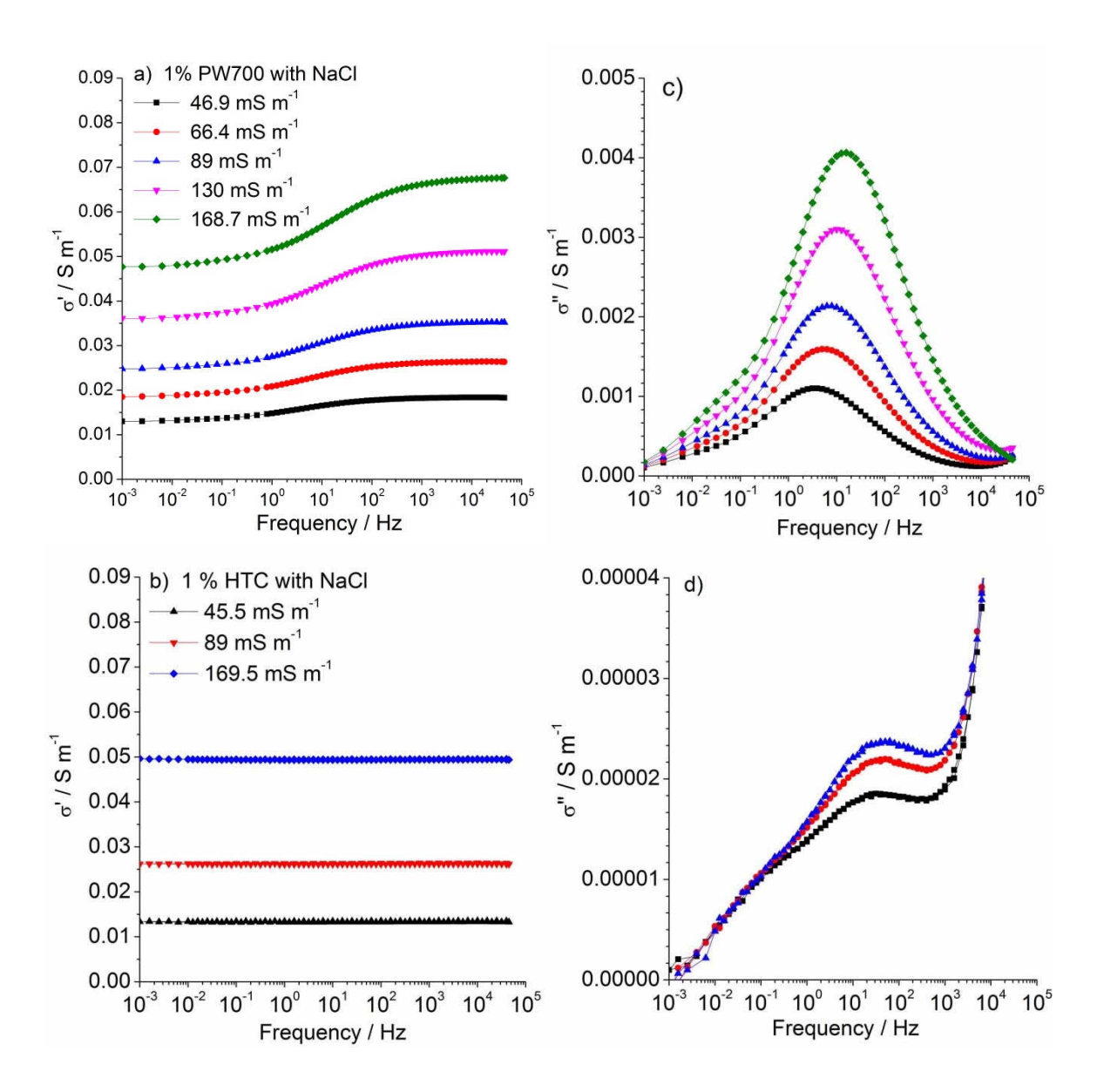


Figure 7. Complex conductivity of 1 % PW700 (a: real part, c: imaginary part) and HTC (b: real part, d: imaginary part) at different concentrations (electrolyte conductivities) of NaCl electrolyte.

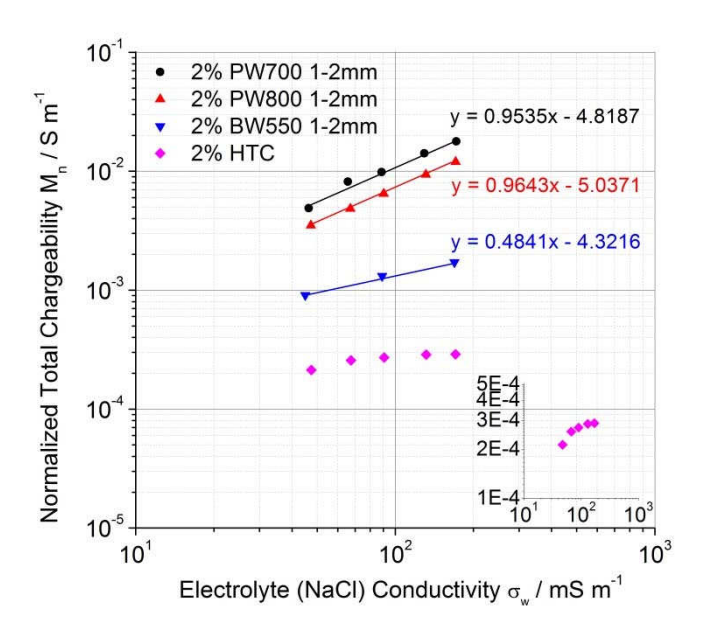


Figure 8. Normalised total chargeability M<sub>n</sub> of mixtures of 2 % PW700, PW800, BW550 and HTC in sand as a function of electrolyte conductivity (NaCl).

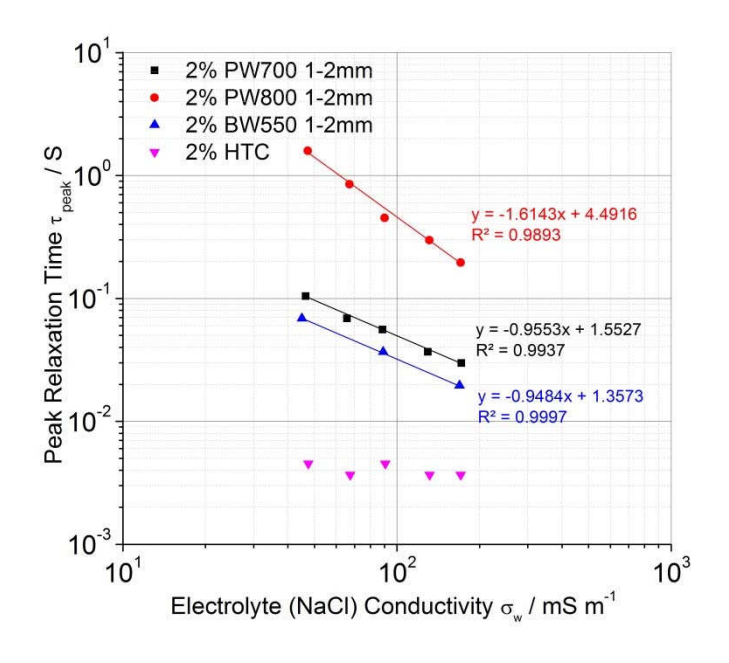


Figure 9. Peak relaxation time  $\tau_{peak}$  of mixtures of 2 % PW700, PW800, BW550 and HTC in sand as a function of electrolyte conductivity (NaCl).

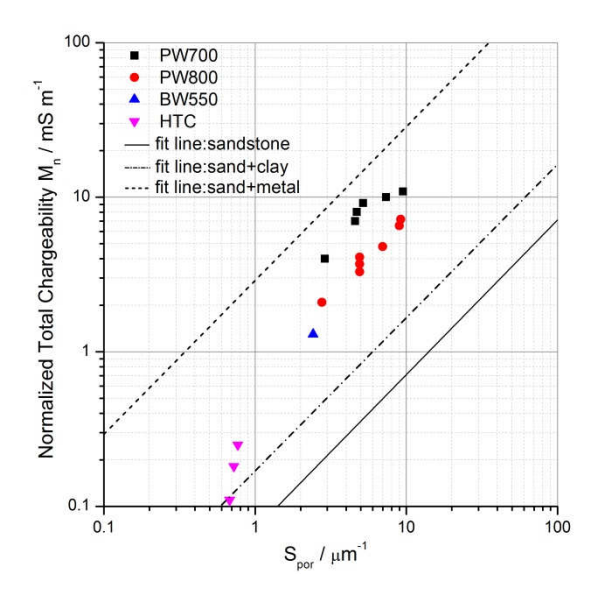


Figure 10. Relationship between normalised total chargeability M<sub>n</sub> derived from DD and the normalised specific surface area S<sub>por</sub> for different sand-biochar mixtures (NaCl electrolyte, 100 mS m<sup>-1</sup>). For comparison, fitting curves for different materials from Weller et al. (2010) are also provided.

## **List of Tables**

Table 1 Chemical composition and BET surface areas of biochars

biochar / Size (mm)	С	Н	N	О	ash	H/C	O/C	A <sub>s</sub> (BET)
	% (w/w)	(molar)	(mass)	$m^2 g^{-1}$				
PW700 / 1-2	77.9	1.70	0.623	13.5	9.1	0.26	0.17	185
PW700 / 0.5-1	71.5	1.68	0.703	14.1	15.3	0.28	0.20	172
PW700 / 0.25-0.5	65.7	1.74	0.593	14.3	19.4	0.32	0.22	173
PW800 / 1-2	82.4	1.77	0.400	11.0	4.2	0.26	0.13	181
PW800 / 0.5-1	81.6	1.95	0.350	11.7	4.8	0.29	0.14	174
PW800 / 0.25-0.5	81.6	2.09	0.430	12.4	4.8	0.31	0.15	174
BW550§	87.5	2.63	0.320	9.6	1.6	0.36	0.11	39
HTC <sup>\$</sup>	50.4	5.09	no data	35.9	5.1	1.21	0.71	5.4

<sup>§</sup> Data for element and ash content taken from Borchard et al. 2014 (Charcoal in that paper)

<sup>§</sup> Data for element and ash content taken from Bai et al. 2014 (htcBC5 in that paper)

Table 2. Parameters of measured samples of sand-biochar mixture

Biochar in	Particle size (mm)	Mass fraction and associated range of pore						
mixture		water conductivity						
		$(mS m^{-1})$						
		0.5 %	1 %	1.5 %	2 %			
PW700	0.25-0.5		47					
	0.5-1		47.4					
	1-2	46.8	46.9 - 168.7	46.9	46.4 - 171.7			
PW800	0.25-0.5		46					
	0.5-1	46	46	47.2	47			
	1-2		46.1		47.3 - 170.8			
BW550	1-2				45-169.1			
HTC	powdery		45.5 – 169.5	47.5	47.5 - 170.7			

# Position suggestion:

Table 1 Position: refer to the section 2: Materials and Methods - Materials

Table 2 Position: refer to the section 2: Materials and Methods - Sample preparation